NANO LETTERS

Letter

pubs.acs.org/NanoLett

Construction of High-Capacitance 3D CoO@Polypyrrole Nanowire Array Electrode for Aqueous Asymmetric Supercapacitor

Cheng Zhou,[†,§] Yangwei Zhang,[†,§,∥] Yuanyuan Li,[*,‡] and Jinping Liu[*,†]

[†]Institute of Nanoscience and Nanotechnology, Department of Physics, Central China Normal University, Wuhan 430079, Hubei, People's Republic of China

[‡]School of Optical and Electronic Information, Huazhong University of Science and Technology, Wuhan, 430074, People's Republic of China

Supporting Information

ABSTRACT: We have developed a supercapacitor electrode composed of well-aligned CoO nanowire array grown on 3D nickel foam with polypyrrole (PPy) uniformly immobilized onto or firmly anchored to each nanowire surface to boost the pseudocapacitive performance. The electrode architecture takes advantage of the high electrochemical activity from both the CoO and PPy, the high electronic conductivity of PPy, and the short ion diffusion pathway in ordered mesoporous nanowires. These merits together with the elegant synergy between CoO and PPy lead to a high specific capacitance of 2223 F g^{-1} approaching the theoretical value, good rate capability, and cycling stability (99.8% capacitance retention after 2000 cycles). An aqueous asymmetric supercapacitor device with a maximum voltage of 1.8 V fabricated by using our hybrid array as the positive electrode and activated carbon film as the negative electrode has demonstrated high energy density (~43.5 Wh kg^{-1}), high power density (~5500 W kg^{-1} at 11.8 Wh kg^{-1}) and outstanding cycleability (~20 000 times). After charging for only ~10 s, two such 4 cm^2 asymmetric supercapacitors connected in series can efficiently power 5 mm diameter red, yellow, and green round LED indicators (lasting for 1 h for red LED) and drive a mini 130 rotation-motor robustly.

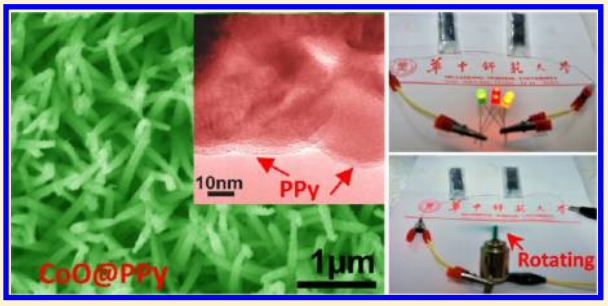

KEYWORDS: *CoO, conducting polymer, hybrid nanowire array, asymmetric supercapacitor*

The increasing demand for energy in the 21st century has triggered tremendous research efforts for energy storage and conversion from clean and renewable energy sources.[1,2] Electrochemical capacitors (ECs) are a promising energy storage device for many portable systems and hybrid electric vehicles due to their high power density, long lifespan, and good pulse charge−discharge characteristics.[1a,b] So far, nanomaterials with high specific surface area have been widely utilized to enhance the charge accumulation and ion transport in ECs. For example, graphene, an emerging ultrathin two-dimensional (2D) carbon material, can enable the ultrafast charging/discharging of electric double-layer capacitor (EDLC);[3,4] ternary transition metal oxide nanostructures can provide multiple redox reactions for pseudocapacitor.[5] Besides, establishment of intriguing nanoarchitectures for EC electrodes is also considered as a fundamental prerequisite to boost the electrochemical performance.[6,7] Recent years have witnessed great progress in the design of additive/binder-free electrode architectures to avoid the "dead surface" in traditional slurry-derived electrode and allow for more efficient charge and mass exchange; those include 3D nanowire/tube arrays,[7−10] coaxial nanostructures,[11−19] mesoporous/macroporous foams,[20−23] free-standing textiles/cloths/papers/monolithics,[24−28] and so forth. Despite that the rate capability and cycle stability could be dramatically promoted in these electrodes,[29,30] a big challenge still remains in further improving the capacitance.

Cobalt-based materials such as cobalt oxides and hydroxides are attractive pseudocapacitive electrode materials because of their high electroactivity and easy processing.[11,23,31−43] ECs with cobalt-based nanostructures can store charge on the electrode surface both through a double layer and via a redox reaction.[11,43] Even considering only the Faradic process, Co_3O_4 and $Co(OH)_2$ have very high theoretical capacitances larger than 3000 F g^{-1}[31] but the reported capacitance values are typically lower than 1000 F g^{-1}.[34−42] The difficulty in approaching the theoretical value is strongly associated with limited ion diffusion within conventional dense electrode film and poor electron transfer due to the semiconducting or even insulating property of cobalt compounds, which make them not fully engaged in the electrochemical reactions. Cobalt monoxide (CoO), another kind of cobalt oxide, is also highly electrochemically active, as unveiled in lithium ion battery application.[44] Nevertheless, the research on its nanostructure fabrication and pseudocapacitive performance has rarely been conducted. Taking CoO as a model system to address the

Received: January 29, 2013
Revised: March 28, 2013

   dx.doi.org/10.1021/nl400378j | *Nano Lett.* XXXX, XXX, XXX−XXX

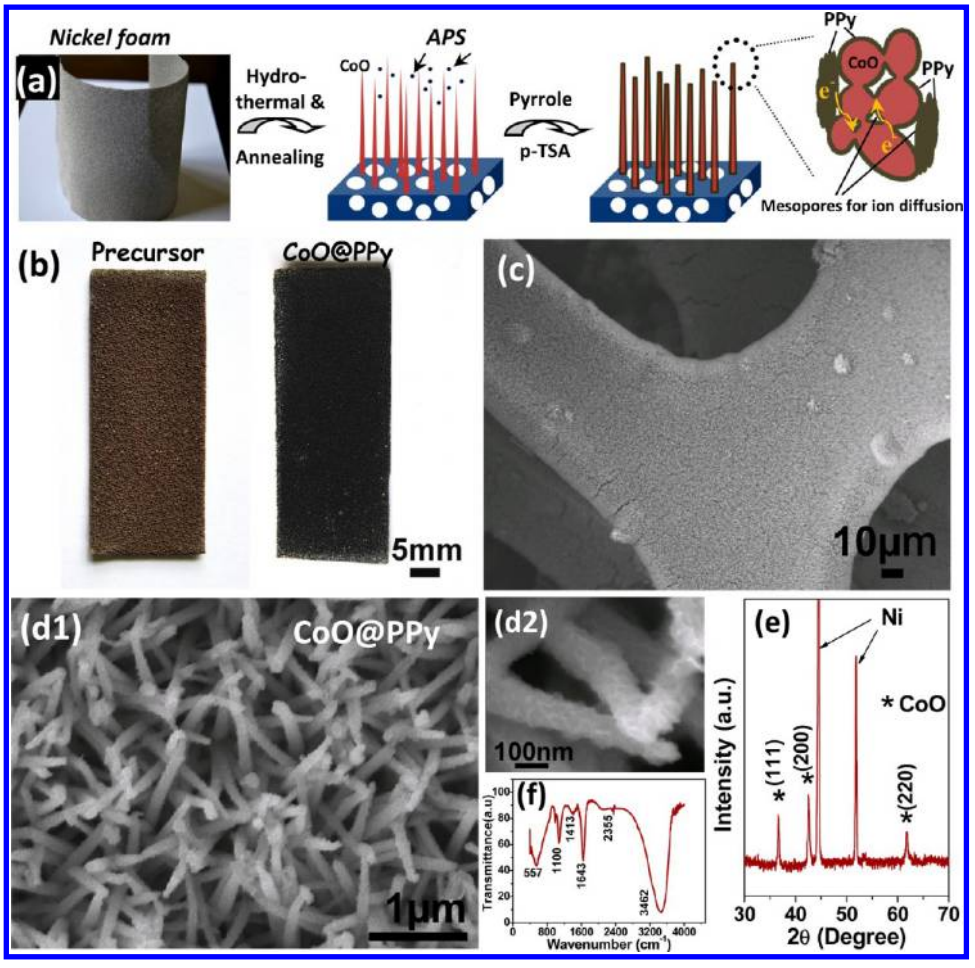

Figure 1. (a) The representative synthetic procedure and structure details of the 3D hybrid nanowire electrode. (b) Optical image of the precursor and CoO@PPy hybrid nanowire array on nickel foam. (c) Low-magnification and (d1,d2) high-magnification SEM images of the hybrid nanowire electrode. (e) XRD pattern and (f) FTIR spectrum of the 3D hybrid nanowire array.

mentioned kinetic issues we have attempted to explore cobalt oxides for potential pseudocapacitive energy storage by elaborately engineering both the electrode configuration and electrical conductivity.

In this Letter, we report a 3D CoO-based nanowire electrode with very high capacitance and good rate capability. To ensure the efficient electrolyte penetration and thus fast ion diffusion, 3D nickel foam with large and uniform macropores, huge supporting area, and high electrical conductivity[32,43] was employed as the current collector; CoO was further grown vertically on the nickel foam and engineered into an quasi-continuous nanowire structure consisting of numerous highly crystalline nanoparticles, leaving a large number of mesopores for ion access and transport. To enhance the conductivity of the 3D electrode, a conducting polymer of polypyrrole (PPy) was integrated into the nanowire array by being either immobilized onto each nanowire surface as a nanosized thin layer or firmly attached to the nanowires in the form of nanoparticulates, while keeping the ordered nanoarchitecture unchanged. PPy was chosen because of its greater density and better degree of flexibility than most other conducting polymers.[45a] Its high electrical conductivity (10−100 S cm^{-1})[45] with respect to that of cobalt oxide (~10^{-2} S cm^{-1}) will definitely lead to significantly improved electron transport within every nanowire. In addition, PPy itself can undergo a fast redox reaction to store charge.[46] As a consequence, the resulting PPy-incorporated 3D nanowire electrode (CoO@PPy) exhibits high specific capacitance of 2223 F g^{-1} at current density of 1 mA cm^{-1} based on the total mass of PPy and CoO (very close to the hybrid's theoretical value of 2467 F g^{-1}) with remarkable areal capacitance at the level of F cm^{-2}. Good rate capability and cycling performance were also demonstrated in such a hybrid array electrode.

To further manifest the potential of the CoO@PPy electrode for practical applications, we have fabricated a 1 × 4 cm^2 1.8 V asymmetric supercapacitor by combining our hybrid array electrode with activated carbon film electrode. Such an asymmetric supercapacitor can deliver maximum energy density and power density of ~43.5 Wh kg^{-1} and 5500 W kg^{-1}, respectively, among the best reported to date for cobalt compound-based asymmetric supercapacitors. With cycle up to 20 000 times, the supercapacitor still remains 91.5% of the initial capacitance. To our best knowledge, our work also presents the first example of the direct hybridization of metal oxide nanostructure arrays with conducting polymer for two-electrode supercapacitor devices.

The representative synthetic procedure of the 3D hybrid nanowire electrode is illustrated in Figure 1a (experimental details are provided in Supporting Information). First, commercial nickel foam was employed as the current collector to grow CoO nanowire array (Figure S1, Supporting Information) via a modified hydrothermal and postannealing

dx.doi.org/10.1021/nl400378j | Nano Lett. XXXX, XXX, XXX−XXX

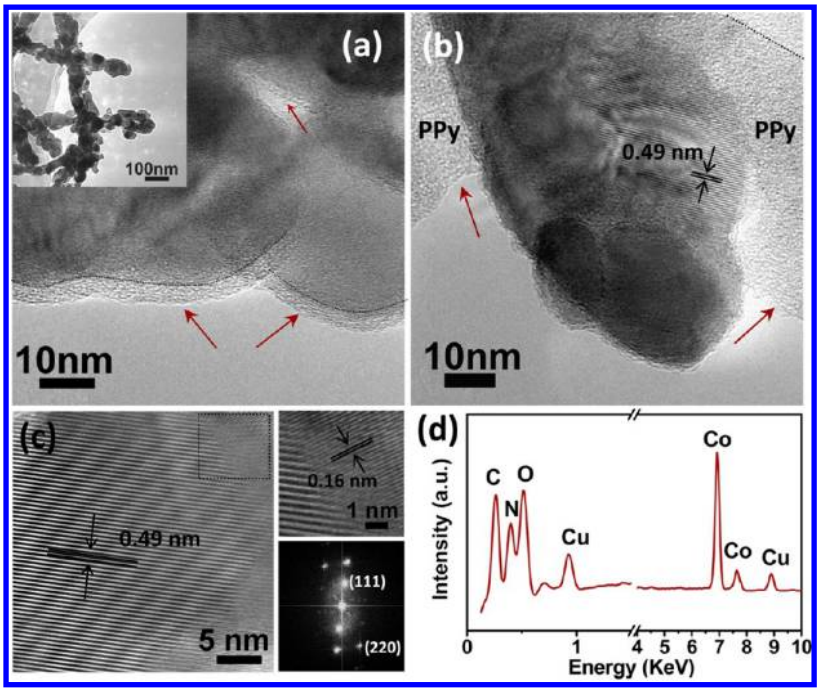

Figure 2. (a, b) HRTEM images of the surface of individual CoO@PPy hybrid nanowires. Inset shows the general view of several nanowires. (c) HRTEM image of the CoO crystal lattice. The enlarged HRTEM image and the corresponding FFT pattern are also shown. (d) EDX result of the hybrid nanowires. Cu signals are from the copper grid.

process.[44] PPy was further immobilized onto the nanowire array based on a simple chemical polymerization by using ammonium persulphate (APS) as the oxidant and *p*-toluenesulfonic acid (*p*-TSA) as the doping agent. The interspaces between neighboring nanowires are believed to enable sufficient solution contact, thus leading to homogeneous PPy modification. The optical images of cobalt hydroxide precursor and final CoO@PPy hybrid nanowire array are shown in Figure 1b. It is apparent that the nanowires can be fabricated on nickel foam on a large scale. Each strip of the nickel foam is fully and uniformly covered by CoO@PPy nanowire array (Figure 1c). Close scanning electron microscopy (SEM) observations reveal that the integration of PPy into the array does not deteriorate the ordered structure (Figure 1d1) but increase the diameter of the nanowires and make the wire surface more wrinkled (Figure 1d2). The X-ray diffraction (XRD) result in Figure 1e unambiguously demonstrates the highly crystalline rock salt cubic structure of CoO nanowires (JCPDS Card No. 48-1719). The Fourier transform infrared spectroscopy (FTIR) spectrum provides further evidence for the presence of PPy (Figure 1f). In detail, the bands at 1643 cm^{-1} should be attributed to the fundamental vibration of pyrrole ring, the peak at 1413 cm^{-1} is due to the =C−H in-plane vibration, and the band at 1100 cm^{-1} is characteristic of the C−N stretching vibration.[46] Two peaks observed at 2355 and 3462 cm^{-1} are associated with the hydroxyl vibration. Finally, the peak at 557 cm^{-1} is attributed to Co−O stretching in CoO.[47] The slight shift of the FTIR peaks of PPy is considered to arise from the interfacial interaction between PPy and CoO.

Chemical polymerization is a universal affordable technique to synthesize conducting polymer powders or to cast them onto 2D planar substrate. Herein, we have successfully extended the method to 3D ordered nanowire arrays for the rational synthesis of uniform 3D ordered hybrid architectures. A typical transmission electron microscopy (TEM) analysis of the hybrid nanowires is displayed in Figure 2a. Obviously, the nanowires consist of quasi-continuous nanoparticles, which typically have a core−shell structure. Each CoO subunit particle is shelled by an amorphous PPy layer with the thickness of several nanometers (see arrows). In addition to being stabilized as a thin shell on the CoO particle surface, some PPy is also attached tightly to the nanowire in the particulate form with apparently larger sizes, as indicated by arrows in Figure 2b (also see Supporting Information Figure S2). High-resolution TEM images in Figure 2b,c reveal two interplanar spacings of 0.49 and 0.16 nm, corresponding to (111) and (220) lattice planes of the face-centered cubic phase CoO, respectively. The highly clear crystal lattice as well as the corresponding well-ordered dot pattern of the fast Fourier transform (FFT) image demonstrates the high-quality single-crystalline nature of CoO. Energy-dispersive X-ray spectroscopy (EDX) analysis (Figure 2d) further indicates that apart from Co and O, elements of C and N can also be detected in the hybrid nanowires, which should be ascribed to the presence of PPy. On the basis of the above characterizations, we can describe the microstructure of CoO@PPy hybrid nanowire, as illustrated in the last picture of Figure 1a. The two kinds of existing PPy in the hybrid structure would definitely facilitate the electron transport and enhance the electrical connection with the current collector. Furthermore, the pores formed between the subunit particles will help facilitate the electrolyte/ion accessibility to nanowires. These two features enable our hybrid electrode to satisfy the critical requirements for ECs.

In order to gain the optimized electrochemical performance of our 3D hybrid nanowire electrode, we have studied the effect of pyrrole monomer concentration on the cyclic voltammetry (CV) curves, electrochemical impedance spectroscopy (EIS) results, and rate capabilities (Figure 3a and Supporting Information Figure S3a−d). With other experimental param-

dx.doi.org/10.1021/nl400378j | *Nano Lett.* XXXX, XXX, XXX−XXX

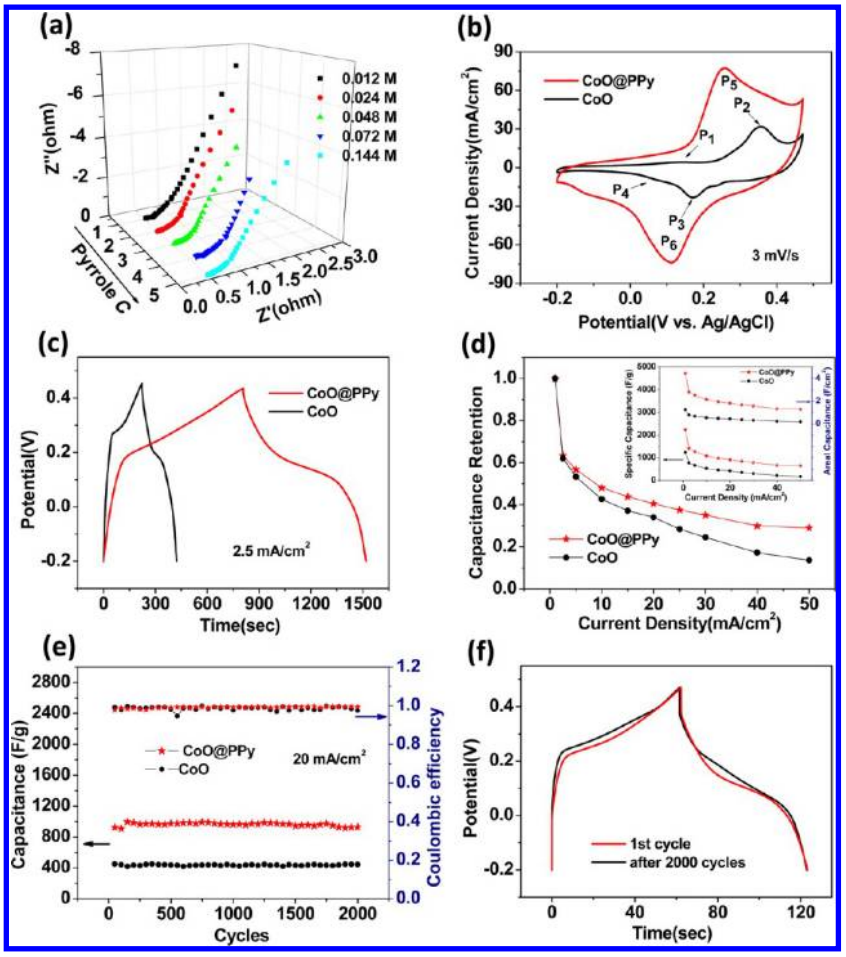

Figure 3. (a) The 3D EIS spectra of the CoO@PPy hybrid electrodes synthesized with different pyrrole concentrations. (b) CV and (c) charge−discharge curve comparisons of the optimized hybrid electrode and the pristine CoO electrode. (d) Capacitance retention rate as a function of current density. The inset is current density dependence of the areal capacitance and specific capacitance for both the CoO@PPy hybrid and pristine CoO nanowire electrodes. (e) Cycling performance of both the two electrodes. (f) Charge−discharge curves of the first and the 2000th cycle for the hybrid nanowire electrode.

eters unchanged, altering the pyrrole concentration can tune the doping (electrical) property and coating amount of PPy. As a consequence, the CVs derived from five samples with various pyrrole concentrations show apparently different integrated areas at the same scan rate. The current of oxidation peak in CV curves first increases and reaches the maximum when pyrrole concentration is 0.072 M. Further increase of pyrrole concentration leads to the oxidation current decreasing (Supporting Information Figure S3a), because the excess PPy could possibly prevent the ion penetration to the inner CoO nanowires. For the EIS spectra (Figure 3a and Supporting Information Figure S3b and c), the five samples all demonstrate similar form with a semicircle at a higher frequency region and a spike at lower frequency. At the high frequency, the intersection of the curve at the real part indicates the resistance of the electrochemical system (R_s, which includes the inherent resistance of the electroactive material, ionic resistance of electrolyte, and contact resistance at the interface between electrolyte and electrode) and the semicircle diameter reflects the charge-transfer resistance (R_{ct}).[12] R_s of the sample from 0.072 M pyrrole (0.6 Ω) is however greater than those of the other four samples (~0.5 Ω) and possibly due to the larger resistance of PPy in this sample an apparent R_{ct} (~0.16 Ω) is also observed. By contrast, sample from 0.048 M pyrrole displays smallest R_{ct} (~0.05 Ω) in addition to the small R_s, indicative of the best electrical conductivity and electroactivity. Supporting Information Figure S3d further demonstrates that samples from 0.048 and 0.024 M pyrrole have better rate capability than those from 0.072, 0.144, and 0.012 M pyrrole. It can be found that 0.048 M is a critical concentration. When the pyrrole concentration is lower than this value, the rate capability increases while increasing the pyrrole concentration. In that case, the electrical conductivity of the sample is improved (see EIS data) while the ion diffusion from solution to CoO may not be essentially influenced by the PPy layer. When the pyrrole concentration is higher than 0.048 M, further increasing the concentration might deteriorate the PPy's electrical conductivity or leads to much more PPy modification that may hinder the ion diffusion to CoO, accordingly, the rate capability becomes worse. On the basis of the above analysis, the sample from 0.048 M pyrrole possess relatively large CV oxidation current, best EIS property, and rate capability. We finally chose the 0.048 M pyrrole sample to perform the following electrochemical tests.

Figure 3b shows the CV curves of both the pristine CoO and the CoO@PPy hybrid nanowire electrodes at scan rate of 3 mV s^{-1} with the electrolyte of 3 M NaOH. For the pristine CoO nanowire array, two pairs of redox peaks can be observed. The first redox couple P_1 and P_4 are due to the Co^{2+}/Co^{3+} reaction, while the second redox couple P_2 and P_3 are attributed to the

dx.doi.org/10.1021/nl400378j | Nano Lett. XXXX, XXX, XXX−XXX

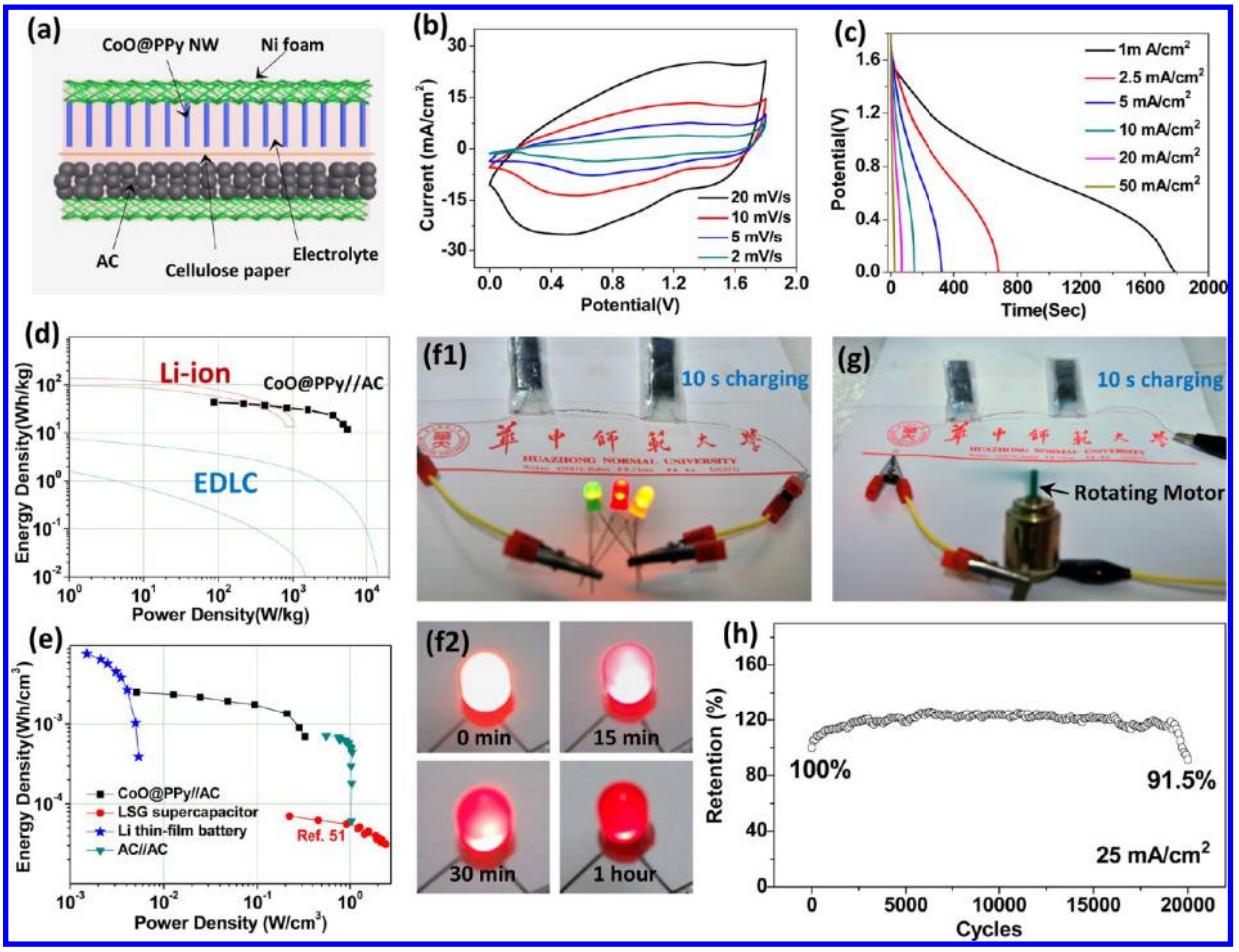

Figure 4. (a) Schematic illustration of the asymmetric supercapacitor configuration. (b) CVs and (c) discharge curves of the asymmetric supercapacitor. (d) Ragone plot of the supercapacitor device. EDLC and Li-ion battery are also included for comparison. (e) Volumetric energy and powder densities of our supercapacitor compared with other data. Data for laser-scribed graphene (LSG) supercapacitor, Li thin-film battery and commercial AC//AC supercapacitor are reproduced with permission from ref 51. (f1) A picture showing that two supercapacitors in series can lighten up three LED indicators. (f2) Images of the red LED at different stages; powered by the 10 s charged supercapacitors. (g) A rotating motor derived by two supercapacitors in series. (h) Cycling stability of our device. After 20 000 cycles, 91.5% capacitance can still be retained.

conversion between Co^{3+} and Co^{4+}.[31] Particularly noteworthy is that after PPy immobilization, the CV curve of the hybrid electrode has drastically expanded, indicating a much larger capacitance. The emergence of only one pair of broad redox peaks P_5 (0.26 V) and P_6 (0.11 V) for the hybrid electrode should result from the superposition of the peaks of the pure CoO electrode and peaks arising from the faradaic redox reaction of PPy via doping/dedoping in alkaline solution (Supporting Information Figure S4a).[46a] Pure and treated (underwent hydrothermal and high temperature postannealing processes) nickel foams were also analyzed independently through CV (Supporting Information Figure S4b). Evidently, the CV integrated areas of the pure and treated nickel foams are both negligible as compared with that of the CoO nanowire electrode, revealing the almost no capacitance contribution of the current collector. Figure 3c further displays the comparison of galvanostatic charge−discharge curves for the pristine and hybrid electrodes at the same current density of 2.5 mA cm^{-2}. As expected, the CoO@PPy hybrid electrode demonstrates much longer discharging time than pristine CoO electrode. The charging and discharging curves are also highly symmetric, evidencing fully reversible electrochemistry. However, it should be noted that the capacitance of the hybrid electrode is not the simple addition of the individual capacitances of pristine CoO array and PPy growing respectively on nickel foam (see the discussion in the caption of Supporting Information Figure S4c). To evaluate the application potential of the 3D hybrid nanowire electrode for ECs, charge−discharge measurements were carried out at various current densities ranging from 1 to 50 mA cm^{-2}. Also presented for comparison are the charge−discharge curves for pristine CoO electrode (Supporting Information Figure S5a,b). The specific capacitance and areal capacitance at these currents as well as the capacitance retention ratio for the two electrodes were calculated and compared, as shown in Figure 3d and its inset. The hybrid structure always exhibits both higher areal and specific capacitances; its discharge areal capacitance is measured to be 4.43 F cm^{-2} at 1 mA cm^{-2}, nearly four times of that of the pristine CoO nanowire electrode (1.23 F cm^{-2}). At higher currents of 5, 10, 20, and 50 mA cm^{-2}, the hybrid electrode still has areal capacitances of 2.51, 2.13, 1.79, and 1.28 F cm^{-2}, respectively. The results are much better than previously reported values from nanostructures fabricated on nickel foam, such as $Ni(OH)_2$ nanosheets (~0.7 F cm^{-2}),[43] Co_3O_4 porous nanowall (~0.52 F cm^{-2} at 3.2 mA cm^{-2})[38] and nanowires (~1.5 F cm^{-2} at 5 mA cm^{-2}).[32] Besides, the areal capacitances presented here are far greater than those of many hybrid nanostructures, for instance, TiO_2/NiO nanotube array (2.9

dx.doi.org/10.1021/nl400378j | Nano Lett. XXXX, XXX, XXX−XXX

mF cm^{-2} at 0.4 mA cm^{-2}),[17] Ni−NiO core−shell inverse opal (7.8−9 mF cm^{-2})[18] and Fe_3O_4−SnO_2 core−shell nanorod film (2.26−7 mF cm^{-2}).[13] Furthermore, a very high specific capacitance of 2223 F g^{-1} is delivered at 1 mA cm^{-2} for the CoO@PPy hybrid electrode, nearly twice that of the pristine CoO electrode (1212 F g^{-1}). The great value surprisingly approaches the theoretical capacitance of the hybrid electrode (~2467 F g^{-1}; calculation details are provided in Supporting Information), which has never been achieved before; the value is also much superior to those of the reported state-of-the-art Co_3O_4 nanostructure films/arrays on 3D current collector (~1500 F g^{-1}).[26,37,39,41] When the discharge rate is increased ten times from 1 to 10 mA cm^{-2}, the hybrid electrode still maintains ~50% of the initial capacitance (~1111.5 F g^{-1}). With further increasing the current density, the capacitance decreasing rate for the hybrid electrode is obviously slower than that of the pristine CoO electrode. Even at the current density as high as 50 mA cm^{-2}, capacitance of ~647 F g^{-1} is retained, which remains comparable with those of most metal oxide pseudocapacitive materials. By contrast, CoO electrode only keeps ~170 F g^{-1} capacitance at 50 mA cm^{-2}.

The dramatic performance improvement after PPy integration can first be attributed to the smaller R_s (0.52 vs 0.89 Ω) and diffusion resistance of the CoO@PPy hybrid electrode as compared to the pure CoO electrode in the EIS (Supporting Information Figure S5c). Intimately covered PPy increases both the electrical conductivity of each CoO nanowire and the electrical contact of CoO with nickel foam current collector, leading to the maximum utilization of CoO during the electrochemical reactions. This is not possible for pristine CoO nanowire as its experimentally observed capacitance is far from the theoretical value of pure CoO (4292 F g^{-1}). In addition, we believe that well-aligned CoO nanowires can in reverse serve as efficient scaffold to ensure the fine distribution of PPy at nanoscale, making them fully electrochemically accessible. Thus, the synergetic contribution from the two promising pseudocapacitive materials (CoO and PPy) together with the merits of 3D porous nanowire array architecture[6] should account for the exceptionally high capacitance and better rate capability of the CoO@PPy hybrid electrode, which are encouraging since our electrode is entirely carbon additive- and binder-free.

The good electrochemical property of the hybrid electrode was further confirmed by the long-term cycling test at 20 mA cm^{-2} (Figure 3e). During the cycling, the specific capacitance of the hybrid electrode is always more than twice that of the pristine CoO electrode. After 2000 cycles, the hybrid electrode shows negligible loss of capacitance (~ 99.8% capacitance retention). This is also evidenced by the almost overlapped charge−discharge curves of the first and the 2000th cycle, as shown in Figure 3f. Furthermore, the hybrid electrode still maintains a good electrochemical reversibility with 99.86% Coulombic efficiency even after 2000 cycles. EIS result (with the expanded view; Supporting Information Figure S5d) clearly reveals that the hybrid electrode exhibits no pronounced impedance change after cycling as compared to the initial fresh hybrid electrode. Even thought the R_{ct} increases from 0 to ~0.1 Ω, it is still very small, indicating that numerous charging−discharging does no substantial damage to our hybrid electrode.

To further evaluate the CoO@PPy hybrid electrode for real application, a 4 cm^2 asymmetric supercapacitor device was made by using the CoO@PPy electrode as the cathode and the activated carbon (AC) film on Ni foam as the anode in 3 M NaOH with one piece of cellulose paper as the separator (Figure 4a). On the basis of a series of comparative experiments, 8 mg of AC film was chosen to balance the two electrodes' capacitance (see Supporting Information Figure S6 for details). Figure 4b exhibits CV curves of the optimized two-electrode supercapacitor device at different scan rates (see Supporting Information Figure S7; the comparative CVs of positive and negative electrodes performed in a three-electrode cell). Unlike the three-electrode electrochemical feature of CoO@PPy hybrid electrode, the device always displays a quasi-rectangular CV geometry as EDLC, indicating a capacitive behavior. The cell voltage is as large as 1.8 V, which is almost twice that of conventional AC-based symmetric capacitors in aqueous electrolytes (0.8−1.0 V). Self-discharge curve of our supercapacitor device (Supporting Information Figure S8) reveals a relatively long self-discharge time of ~15 h (from V_{max} to $1/2V_{max}$). Galvanostatic discharge curves of the supercapacitor device at various current densities were further illustrated in Figure 4c. The rate capability is also shown in Supporting Information Figure S9. On the basis of these data, Ragone plot of the device describing the relation between energy density and power density was obtained and shown in Figure 4d. Data of traditional lithium ion batteries (LIBs) and EDLC were also provided for comparison. The energy and power densities (E and P) were calculated using equations $E = (\int IV(t)dt)/(m)$ and $P = E/\Delta t$, where I is the discharging current, $V(t)$ is discharging voltage excluding the IR drop, dt is time differential, m is the total mass of the two active electrode materials, and Δt is the discharging time. Our asymmetric supercapacitor displays a high energy density of 43.5 Wh kg^{-1} at a power density of 87.5 W kg^{-1}, approaching the lower end of LIBs. Even at a high power density of 5500 W kg^{-1} (400 mA), the device still has an energy density of 11.8 Wh kg^{-1}, much superior to that of EDLC at the same power level. It is worth noting that very little attention has been paid to asymmetric supercapacitor device performance of cobalt oxides. Therefore, only several data from cobalt-based oxides were available for comparison.[48−50] Our CoO@PPy//AC device exhibits superior performance to other cobalt oxide-based asymmetric supercapacitors, such as Ni−Co oxide/graphene//AC (7.6 Wh kg^{-1} at 5600 W kg^{-1})[49] in which highly conductive graphene was even involved, placing it among the top performing Co-oxide devices. The energy and power densities of our supercapacitor are also higher than those of Ni$(OH)_2$/graphene//RGO (31 Wh kg^{-1} at 420 W kg^{-1})[50] and comparable to those of Ni$(OH)_2$-CNTs//AC (32.5 Wh kg^{-1} at 1800 W kg^{-1}).[43] The volumetric energy and powder densities of our supercapacitor are further shown in Figure 4e and compared with other data. It can be seen that the supercapacitor bridges the performance gap between Li thin-film battery and EDLCs (LSG supercapacitor[51] and commercial AC//AC supercapacitor). However, the volumetric energy and powder densities are largely limited by the use of nickel foam and the performance values can be further improved if alternative current collector having much smaller pore size/volume (still can support microsize thickness nanowire array growth) can be used. We assembled two supercapacitors in series, and after charging for only 10 s to ~3.2 V, the device could power 5 mm diameter red (1.8 V, 20 mA), yellow (2.1 V, 20 mA), and green (2.3 V, 20 mA) round light-emitting diode (LED) indicators efficiently (Figure 4f1,f2). For example, the red LED still remained very bright after 30 min and even effective enough for indication after one hour. More strikingly,

dx.doi.org/10.1021/nl400378j | Nano Lett. XXXX, XXX, XXX−XXX

the device can drive a mini 130 rotation motor (3 V, 0.45 W) robustly after seconds of charging (Figure 4g and Movie in Supporting Information). Figure 4h reveals the outstanding cycling life of our supercapacitor device up to 20 000 times, which has rarely been demonstrated for aqueous electrolyte-based asymmetric supercapacitors. The capacitance increase during the first 5000 cycles is likely due to an "activation process".[42,49] When the cycling approaches 20 000 times, the capacitance suddenly drops because of the destruction of the electrode film after numerous harsh redox reactions.

In summary, 3D CoO@PPy hybrid nanowire array on nickel foam has been developed with outstanding pseudocapacitive performance. The smart synergetic contribution from the CoO nanowires and conductive PPy accounts for the high specific capacitance of 2223 F g^{-1} and the superior cycling stability. In addition, good electrical conductivity rendered by PPy integration, in combination with facile ion diffusion path provided by both the 3D macroporous nickel foam and the mesoporous nanowires, gives rise to enhanced rate capability. Two-electrode asymmetric supercapacitor based on CoO@PPy hybrid electrode further delivers high specific energy and power densities and exhibits outstanding cycling life. Our work not only opens up the possibility to engineer cobalt oxides into a promising pseudocapacitive material but also presents a new and affordable general approach to design hybrid electrode architectures for energy storage devices.

■ ASSOCIATED CONTENT

Supporting Information

Experimental details and additional supporting data. This material is available free of charge via the Internet at http://pubs.acs.org.

■ AUTHOR INFORMATION

Corresponding Author

*E-mail: (J.L.) liujp@phy.ccnu.edu.cn; (Y.L.) liyynano@yahoo.com.cn.

Present Address

[‖](Y.Z.) International Center for Quantum Materials, Peking University, Beijing 100871, People's Republic of China.

Author Contributions

[§]C.Z. and Y.Z. contributed equally to this work

Notes

The authors declare no competing financial interest.

■ ACKNOWLEDGMENTS

This work was supported by grants from the National Natural Science Foundation of China (No. 51102105, 11104088) and Self-determined Research Funds of CCNU from the Colleges' Basic Research and Operation of MOE (CCNU12A01009). Thanks to Professor Liqiang Mai at WUT-Harvard Joint Nano Key Laboratory, Wuhan University of Technology for strong support and stimulating discussion.

■ REFERENCES

(1) (a) Miller, J. R.; Simon, P. *Science* **2008**, *321*, 651. (b) Simon, P.; Gogotsi, Y. *Nat. Mater.* **2008**, *7*, 845. (c) Wang, Y.; Cao, G. Z. *Adv. Mater.* **2008**, *20*, 2251. (d) Liu, J.; Cao, G. Z.; Yang, Z. G.; Wang, D. H.; Dubois, D.; Zhou, X. D.; Graff, G. L.; Pederson, L. R.; Zhang, J. G. *ChemSusChem* **2008**, *1*, 676.

(2) (a) Tian, B.; Kempa, T. J.; Lieber, C. M. *Chem. Soc. Rev.* **2009**, *38*, 16. (b) Tian, B.; Zheng, X.; Kempa, T. J.; Fang, Y.; Yu, N.; Yu, G.; Huang, J.; Lieber, C. M. *Nature* **2007**, *449*, 885. (c) Gogotsi, Y.; Simon, P. *Science* **2011**, *334*, 917.

(3) (a) Yoo, J. J.; Balakrishnan, K.; Huang, J. S.; Meunier, V.; Sumpter, B. G.; Srivastava, A.; Conway, M.; Reddy, A. L. M.; Yu, J.; Vajtai, R.; Ajayan, P. M. *Nano Lett.* **2011**, *11*, 1423. (b) Stoller, M. D.; Park, S. J.; Zhu, Y. W.; An, J. H.; Ruoff, R. S. *Nano Lett.* **2008**, *8*, 3498. (c) Yu, G.; Hu, L.; Liu, N.; Wang, H.; Vosgueritchian, M.; Yang, Y.; Cui, Y.; Bao, Z. *Nano Lett.* **2011**, *11*, 4438.

(4) (a) Cheng, Y. W.; Lu, S. T.; Zhang, H. B.; Varanasi, C. V.; Liu, J. *Nano Lett.* **2012**, *12*, 4206. (b) Zhu, Y. W.; Murali, S.; Stoller, M. D.; Ganesh, K. J.; Cai, W. W.; Ferreira, P. J.; Pirkle, A.; Wallace, R. M.; Cychosz, K. A.; Thommes, M.; Su, D.; Stach, E. A.; Ruoff, R. S. *Science* **2011**, *332*, 1537.

(5) Wei, T. Y.; Chen, C. H.; Chien, H. C.; Lu, S. Y.; Hu, C. C. *Adv. Mater.* **2010**, *22*, 347.

(6) Jiang, J.; Li, Y. Y.; Liu, J. P.; Huang, X. T.; Yuan, C. Z.; Lou, X. W. *Adv. Mater.* **2012**, *24*, 5166.

(7) Jiang, J.; Li, Y. Y.; Liu, J. P.; Huang, X. T. *Nanoscale* **2011**, *3*, 45.

(8) Hu, C. C.; Chang, K. H.; Lin, M. C.; Wu, Y. T. *Nano Lett.* **2006**, *6*, 2690.

(9) (a) Liu, B.; Zhang, J.; Wang, X. F.; Chen, G.; Chen, D.; Zhou, C. W.; Shen, G. Z. *Nano Lett.* **2012**, *12*, 3005. (b) Guo, W. X.; Xue, X. Y.; Wang, S. H.; Lin, C. J.; Wang, Z. L. *Nano Lett.* **2012**, *12*, 2520.

(10) (a) Lu, X. H.; Zhai, T.; Zhang, X. H.; Shen, Y. Q.; Yuan, L. Y.; Hu, B.; Gong, L.; Chen, J.; Gao, Y. H.; Zhou, J.; Tong, Y. X.; Wang, Z. L. *Adv. Mater.* **2012**, *24*, 938. (b) Lu, X. H.; Wang, G. M.; Zhai, T.; Yu, M. H.; Gan, J. Y.; Tong, Y. X.; Li, Y. *Nano Lett.* **2012**, *12*, 1690. (c) Li, Q.; Wang, Z. L.; Li, G. R.; Guo, R.; Ding, L. X.; Tong, Y. X. *Nano Lett.* **2012**, *12*, 3803.

(11) Liu, J. P.; Jiang, J.; Cheng, C. W.; Li, H. X.; Zhang, J. X.; Gong, H.; Fan, H. J. *Adv. Mater.* **2011**, *23*, 2076.

(12) Liu, J. P.; Jiang, J.; Bosman, M.; Fan, H. J. *J. Mater. Chem.* **2012**, *22*, 2419.

(13) Li, R. Z.; Ren, X.; Zhang, F.; Du, C.; Liu, J. P. *Chem. Commun.* **2012**, *48*, 5010.

(14) Jiang, J.; Liu, J. P.; Zhou, W. W.; Zhu, J. H.; Huang, X. T.; Qi, X. Y.; Zhang, H.; Yu, T. *Energy Environ. Sci.* **2011**, *4*, 5000.

(15) Liu, J. P.; Cheng, C. W.; Zhou, W. W.; Li, H. X.; Fan, H. J. *Chem. Commun.* **2011**, *47*, 3436.

(16) Mai, L. Q.; Yang, F.; Zhao, Y. L.; Xu, X.; Xu, L.; Luo, Y. Z. *Nat. Commun.* **2011**, *2*, 381.

(17) Kim, J. H.; Zhu, K.; Yan, Y. F.; Perkins, C. L.; Frank, A. J. *Nano Lett.* **2010**, *10*, 4099.

(18) Kim, J. H.; Kang, S. H.; Zhu, K.; Kim, J. Y.; Neale, N. R.; Frank, A. J. *Chem. Commun.* **2011**, *47*, 5214.

(19) Bao, L. H.; Zang, J. F.; Li, X. D. *Nano Lett.* **2011**, *11*, 1215.

(20) Zhang, H. G.; Yu, X. D.; Braun, P. V. *Nat. Nanotechnol.* **2011**, *6*, 277.

(21) Lang, X. Y.; Hirata, A.; Fujita, T.; Chen, M. W. *Nat. Nanotechnol.* **2011**, *6*, 232.

(22) Meng, F.; Ding, Y. *Adv. Mater.* **2011**, *23*, 4098.

(23) Guan, C.; Li, X. L.; Wang, Z. L.; Cao, X. H.; Soci, C.; Zhang, H.; Fan, H. J. *Adv. Mater.* **2012**, *24*, 4186.

(24) Sheng, K. X.; Sun, Y. Q.; Li, C.; Yuan, W. J.; Shi, G. Q. *Sci. Rep.* **2012**, *2*, 247.

(25) Kaempgen, M.; Chan, C. K.; Ma, J.; Cui, Y.; Gruner, G. *Nano Lett.* **2009**, *9*, 1872.

(26) Chen, W.; Rakhi, R. B.; Hu, L.; Xie, X.; Cui, Y.; Alshareef, H. N. *Nano Lett.* **2011**, *11*, 5165.

(27) Meng, C. Z.; Liu, C. H.; Chen, L. Z.; Hu, C. H.; Fan, S. S. *Nano Lett.* **2010**, *10*, 4025.

(28) Wang, K.; Wu, H. P.; Meng, Y. N.; Zhang, Y. J.; Wei, Z. X. *Energy Environ. Sci.* **2012**, *5*, 8384.

(29) Liu, R.; Lee, S. B. *J. Am. Chem. Soc.* **2008**, *130*, 2942.

(30) Liu, R.; Duay, J.; Lane, T.; Lee, S. B. *Phys. Chem. Chem. Phys.* **2010**, *12*, 4309.

(31) Cao, L.; Xu, F.; Liang, Y. Y.; Li, H. L. *Adv. Mater.* **2004**, *16*, 1853.

(32) Huang, J. C.; Zhu, J. T.; Cheng, K.; Xu, Y.; Cao, D. X.; Wang, G. L. *Electrochim. Acta* **2012**, *75*, 273.
(33) Li, Y. G.; Hasin, P.; Wu, Y. Y. *Adv. Mater.* **2010**, *22*, 1926.
(34) Gupta, V.; Kusahara, T.; Toyama, H.; Gupta, S.; Miura, N. *Electrochem. Commun.* **2007**, *9*, 2315.
(35) Hosono, E.; Fujihara, S.; Honma, I.; Ichihara, M.; Zhou, H. *J. Power Sources* **2006**, *158*, 779.
(36) Wei, T. Y.; Chen, C. H.; Chang, K. H.; Lu, S. Y.; Hu, C. C. *Chem. Mater.* **2009**, *21*, 3228.
(37) Wang, H. T.; Zhang, L.; Tan, X. H.; Holt, C. M. B.; Zahiri, B.; Olsen, B. C.; Mitlin, D. *J. Phys. Chem. C* **2011**, *115*, 17599.
(38) Wu, J. B.; Lin, Y.; Xia, X. H.; Xu, J. Y.; Shi, Q. Y. *Electrochim. Acta* **2011**, *56*, 7163.
(39) Qing, X. X.; Liu, S. Q.; Huang, K. L.; Lv, K. Z.; Yang, Y. P.; Lu, Z. G.; Fang, D.; Liang, X. X. *Electrochim. Acta* **2011**, *56*, 4985.
(40) Yang, L.; Cheng, S.; Ding, Y.; Zhu, X. B.; Wang, Z. L.; Liu, M. L. *Nano Lett.* **2012**, *12*, 321.
(41) Zhang, F.; Yuan, C. Z.; Lu, X. J.; Zhang, L. J.; Che, Q.; Zhang, X. G. *J. Power Sources* **2012**, *203*, 250.
(42) Rakhi, R. B.; Chen, W.; Cha, D. K.; Alshareef, H. N. *Nano Lett.* **2012**, *12*, 2559.
(43) Tang, Z.; Tang, C. H.; Gong, H. *Adv. Funct. Mater.* **2012**, *22*, 1272.
(44) Jiang, J.; Liu, J. P.; Ding, R. M.; Ji, X. X.; Hu, Y. Y.; Li, X.; Hu, A. Z.; Wu, F.; Zhu, Z. H.; Huang, X. T. *J. Phys. Chem. C* **2010**, *114*, 929.
(45) (a) Snook, G. A.; Kao, P.; Best, A. S. *J. Power Sources* **2011**, *196*, 1. (b) Kuwabata, S.; Nakamura, J.; Yoneyama, H. *J. Electrochem. Soc.* **1990**, *137*, 2147.
(46) (a) An, K. H.; Jeon, K. K.; Heo, J. K.; Lim, S. C.; Bae, D. J.; Lee, Y. H. *J. Electrochem. Soc.* **2002**, *149*, A1058. (b) Zhang, X.; Yang, W. S.; Ma, Y. W. *Electrochem. Solid-State Lett.* **2009**, *12*, A95.
(47) Lenglet, M.; Lopitaux, J.; Terrier, L.; Chartier, P.; Koenig, J. F.; Nkeng, E.; Poillerat, G. *J. Phys. IV* **1993**, *03*, C9−477.
(48) Xiao, J. W.; Yang, S. H. *J. Mater. Chem.* **2012**, *22*, 12253−12262.
(49) Wang, H. L.; Holt, C. M. B.; Li, Z.; Tan, X. H.; Amirkhiz, B. S.; Xu, Z. W.; Olsen, B. C.; Stephenson, T.; Mitlin, D. *Nano Res.* **2012**, *5* (9), 605−617.
(50) Wang, H. L.; Liang, Y. Y.; Mirfakhrai, T.; Chen, Z.; Casalongue, H. S.; Dai, H. J. *Nano Res.* **2011**, *4*, 729.
(51) El-Kady, M. F.; Strong, V.; Dubin, S.; Kaner, R. B. *Science* **2012**, *335*, 1326.

dx.doi.org/10.1021/nl400378j | *Nano Lett.* XXXX, XXX, XXX−XXX